SEECCM III
3rd South-East European Conference on Computational Mechanics-
an ECCOMAS and IACM Special Interest Conference
M. Papadrakakis, M. Kojic, I. Tuncer (eds.)
Kos Island, Greece, 12–14 June 2013

REDUCED ORDER MODELLING OF HIGH-FIDELITY COMPUTATIONAL FLUID-STRUCTURE INTERACTION ANALYSIS FOR AEROELASTIC SYSTEMS

Pınar Acar[1] **and Melike Nikbay**[2]

[1], [2] Istanbul Technical University, Maslak, Istanbul, 34469, Turkey
e-mail: acarpin@itu.edu.tr, nikbay@itu.edu.tr

Keywords: Aeroelasticity, Fluid-Structure Interaction, Reduced Order Modelling, Polynomial Chaos Expansion, Proper Orthogonal Decomposition, HIRENASD, S^{4}T.

Abstract. *We investigate model reduction techniques through computational aeroelastic analyses of the HIRENASD and S^{4}T wings. The aim of the present work is to construct accurate and computationally efficient reduced order models for high-fidelity aeroelastic computations. Firstly, the aeroelastic analyses of the specified wings are performed by high-fidelity structural and aerodynamic models to substantiate the fluid-structure interaction. Concerning high amount of computational time required to perform such high-fidelity fluid-structure interaction analyses, the model orders are reduced by introducing relevant reduction techniques such as Polynomial Chaos Expansion and Proper Orthogonal Decomposition. The final aeroelastic analyses performed on these reduced models agree well with the initial high-fidelity computational analyses.*

1 INTRODUCTION

Model reduction is a powerful numerical approach and has been applied to many disciplines such as fluid dynamics, aeroelasticity, structural dynamics and control. In general, the complex high-fidelity numerical models accurately represent the problem. However, in many cases, a burden of computational time is required to achieve the solution. When this is the case, it is nearly impossible to perform some applications requiring great amount of computational efforts such as uncertainty quantification and multidisciplinary optimization. The reduced models can successfully represent the full model with an optimal basis. Thus, they can save great amount of computational time and effort while modelling the problem and finding its solutions. In the present work, the reduced modelling strategy is used to represent the high-fidelity computational models of the HIRENASD and S^4T wings to perform static aeroelastic and flutter analyses. The major anticipation from the constructed reduced models is to present accurate solutions while providing a considerable reduction in the computational time. The fundamental steps of the reduced order modelling (ROM) strategy of this work starts with the construction of the high-fidelity computational models. These computational models are developed to perform static aeroelastic analyses of the HIRENASD and S^4T wings, and flutter analysis of the S^4T wing in ZEUS software. ZEUS is an Euler Unsteady Aerodynamic Solver developed for aeroelastic solutions of complex geometries [1]. It involves automated mesh generation scheme and overset grid capability for complex configurations while using Cartesian grid and employing boundary layer coupling. It also uses modal data importer and ZAERO 3D spline module, and constructs structural grids. ZEUS uses central difference with JST (Jameson-Schmidt-Turkel) Artificial Dissipation Scheme for flux construction and Green's Integral Boundary Layer Method for turbulence model [1]. Aeroelastic analyses in ZEUS require the own input file and modal solution from the finite element solver. In the present work, Nastran is used as the structural solver for the modal analysis. Aerodynamic mesh is generated and Fluid Structure Interaction (FSI) is provided in ZEUS to perform the required aeroelastic analyses after importing the modal solution. Once the aeroelastic analyses are accomplished for the reference cases, they should be repeated based on the design samples generated to construct the reduced models. After generating an adequate number of sampling, the model reduction is performed by using non-intrusive Polynomial Chaos Expansion (PCE) and Proper Orthogonal Decomposition (POD) methods. Both the PCE and POD methods aim to ameliorate the computational efficiency.

The origin of the PCE is based on homogenous chaos theory of Wiener [2]. The PCE represents the high-fidelity model in terms of generalized orthogonal functions [3]. It estimates coefficients of these orthogonal polynomials based on a set of response function evaluations and makes use of sampling and linear regression. In literature, the PCE method is generally used to quantify uncertainties in a computational problem. For example, Eldred and Burkardt [4] investigated the non-intrusive PCE method to quantify the uncertainties in different example problems and compared its results with Stochastic Collocation Method. Witteveen and Bijl [5] applied PCE to the problems with nonlinear input variables and compared their results with Monte Carlo Simulation (MCS) method. Reduced models are useful for examining responses near the mean values. However, they are not capable of predicting responses with large variations in the input [6]. With an exception, the PCE method allows large variations in the input parameters and is far more efficient than MCS [7]. In the present work, the PCE method is used to construct reduced models in order to investigate its accuracy when small variations are considered. The results of the PCE are then compared to the results of the POD based reduced models and the high-fidelity computational models.

The POD method, which is also known as Karhunen-Loeve decomposition [8, 9] or principal component analysis [10], is an efficient method that has been widely utilized for model reduction of large-scale systems [11]. It defines the given higher-order system as a linear combination of independent and orthogonal basis functions. The POD method has numerous application areas such as fluid dynamics [12, 13], aeroelasticity [14, 15] and design optimization [16, 17]. This method is an extension of the numerical technique known as Singular Value Decomposition (SVD). For example, Chatterjee [18] discussed POD and SVD with their applications to two example problems: low-rank approximations of a surface and a posteriori analysis of data from a simulated vibroimpact system respectively. The first example problem of his study is also used as a benchmark problem in the present work for validation purpose. Pinnau [19] applied POD method to a heat transfer problem specified by a nonlinear parabolic partial differential equation. Zhang et. al [20] applied POD method to the study of the aerodynamics of a membrane wing under the MAV flight condition. The choice of the data set plays a crucial role to construct reduced models based on POD method. There are different techniques to apply the POD method such as balanced POD [11] and constrained POD scheme [21]. However, the most prominent is the method of snapshots introduced by Sirovich [22], which is also the main approach of the POD method in the present work. In this method, the data set is chosen as snapshots that include the spatial distribution of a numerical simulation and should reflect the system characteristics.

In the final step of the present work, the static aeroelastic and flutter analyses of the HIRENASD and S^4T wings are performed for the reference cases by using the PCE and POD based reduced models. Then, the accuracies of the reduced models are compared to the high-fidelity computational models. Both the PCE and POD methods give satisfactory results while their accuracies will be investigated in a more detailed manner throughout the present work. But first, the theoretical background of the FSI will be discussed and then the computational aeroelastic models for the HIRENASD and S^4T wings will be introduced. After completing the aeroelastic analyses based on the reference data, the main focus of the present study will be on model reduction strategy and applications.

2 THEORETICAL BACKGROUND

The present work firstly concentrates on the static aeroelastic analyses of the HIRENASD and S^4T wings, and flutter analysis of the S^4T wing. All the aeroelastic analyses require structural and aerodynamic modelling, and FSI to determine the output parameters. Here, the aerodynamic modelling and FSI are constructed by using ZEUS software.

ZEUS is ZONA's Euler Unsteady Aerodynamic Solver that integrates the essential disciplines required for aeroelastic design and analysis [23]. It uses an Euler equation solver with/without viscous effects as the underlying aerodynamic force generator coupled with the structural finite element modal solution to solve various aeroelastic problems such as flutter, maneuver loads, store ejection loads, gust loads, and static aeroelastic/trim analysis. In the present work, the modal solutions for the HIRENASD and S^4T wings are based on NASA's structural models developed in Nastran software.

The Euler equation solver of ZEUS employs the Euler equations on a Cartesian grid system using a cell-centered finite volume method with dual-time stepping algorithm for unsteady solutions. The viscous effects are included by coupling the Euler solution with a steady boundary-layer equation. For turbulence closure, the Green's lag entrainment is employed. Because of solving the Euler equations with boundary layer coupling, the requirement of large computing resources by a Navier-Stokes code can be avoided by ZEUS. Therefore, ZEUS provides a good

balance between the complete modelling of the flow physics and the computational efficiency [23].

2.1 Unsteady Euler Solver on Stationary Cartesian Grid

ZEUS is an unsteady aerodynamics generator based on a stationary Cartesian grid. It solves the time-accurate Euler equations using a cell-centered central-differencing finite-volume method with JST artificial dissipation scheme [24] implemented for stability of the flow solver [23].

2.1.1 Time-Accurate Euler Method

The three-dimensional unsteady Euler equations in conservative differential form and in curvilinear coordinates can be defined as follows:

$$\frac{\partial Q}{\partial t} + \frac{\partial H_1}{\partial \xi} + \frac{\partial H_2}{\partial \eta} + \frac{\partial H_3}{\partial \zeta} = 0 \tag{1}$$

where Q is the product of conservative flow variables vector, q, and the inverse of the transformation Jacobian, J. H_1, H_2 and H_3 are convective fluxes in three curvilinear coordinate directions where:

$$Q = Jq = J \begin{bmatrix} \rho \\ \rho u \\ \rho v \\ \rho w \\ e \end{bmatrix}; \quad H_1 = J \begin{bmatrix} \rho U \\ \rho u U + p\xi_x \\ \rho v U + p\xi_y \\ \rho w U + p\xi_z \\ (e+p)\,U - p\xi_t \end{bmatrix}$$

$$H_2 = J \begin{bmatrix} \rho V \\ \rho u V + p\eta_x \\ \rho v V + p\eta_y \\ \rho w V + p\eta_z \\ (e+p)\,V - p\eta_t \end{bmatrix}; \quad H_3 = J \begin{bmatrix} \rho W \\ \rho u W + p\zeta_x \\ \rho v W + p\zeta_y \\ \rho w W + p\zeta_z \\ (e+p)\,W - p\zeta_t \end{bmatrix}$$

U, V, W and u, v, w are the three components of the flow velocity in curvilinear and Cartesian coordinates, respectively.

2.2 Computational Aeroelastic Analysis

The computational aeroelastic analysis requires the interaction between the structural modal solution of Nastran and the aerodynamic model constructed in ZEUS. The FSI is also provided in ZEUS software to perform both static aeroelastic and flutter analyses. For a general aeroelastic system, the time-dependent equations of motion can be defined as shown below:

$$[M]\{\ddot{u}\} + [C]\{\dot{u}\} + [K]\{u\} = \{F_a\} + \{F_e\} \tag{2}$$

where $[M]$, $[C]$ and $[K]$ are generalized mass, damping and stiffness matrices while $[F_a]$ shows steady forces matrix, $[F_e]$ denotes time-dependent external forces matrix and $\{u\}$ is the displacement vector. The above equation must be considered for the flutter analyses. However, the time dependent terms and external forces should be omitted for static aeroelastic analyses:

$$[K]\{u\} = \{F_a\} \tag{3}$$

3 COMPUTATIONAL AEROELASTIC ANALYSES OF THE HIRENASD AND S^{4}T WINGS

The static aeroelastic and flutter analyses of the HIRENASD and S^{4}T wings are accomplished in ZEUS. The aeroelastic analyses concentrate on the calculation of steady aerodynamic coefficients for both the HIRENASD and S^{4}T wings, and also determination of the flutter boundaries of the S^{4}T wing. In the following two sections, these analyses and outcomes will be evaluated in more details.

3.1 Static Aeroelastic Analysis of the HIRENASD Wing

The first application of this section is the static aeroelastic analysis of the HIRENASD (HIgh REynolds Number Aero-Structural Dynamics) wing to determine steady aerodynamic coefficients. The HIRENASD project was initiated at RWTH Aachen University in 2004. The main purpose of this project is to analyze steady and unsteady aeroelastic experiments in transonic flight regime with a supercritical elastic wing model [25]. The HIRENASD wind-tunnel model was tested in the European Transonic Windtunnel (ETW) in 2006 by Aachen University's Department of Mechanics with funding from the German Research Foundation [26]. The test medium of ETW is nitrogen gas under cryogenic conditions [25]. The wing has a 34^{o} degree of backward sweep angle and a supercritical wing profile BAC 3-11. The aerodynamic reference area is $0.3926\ m^2$ while the mean chord length is $0.3445\ m$ [25]. The HIRENASD wing model planform and assembly are illustrated in Fig.1. Further explanations and elaborations for the wing properties, computational models used to perform the aeroelastic analyses, and static response data can be found in the former study of Nikbay et. al [27].

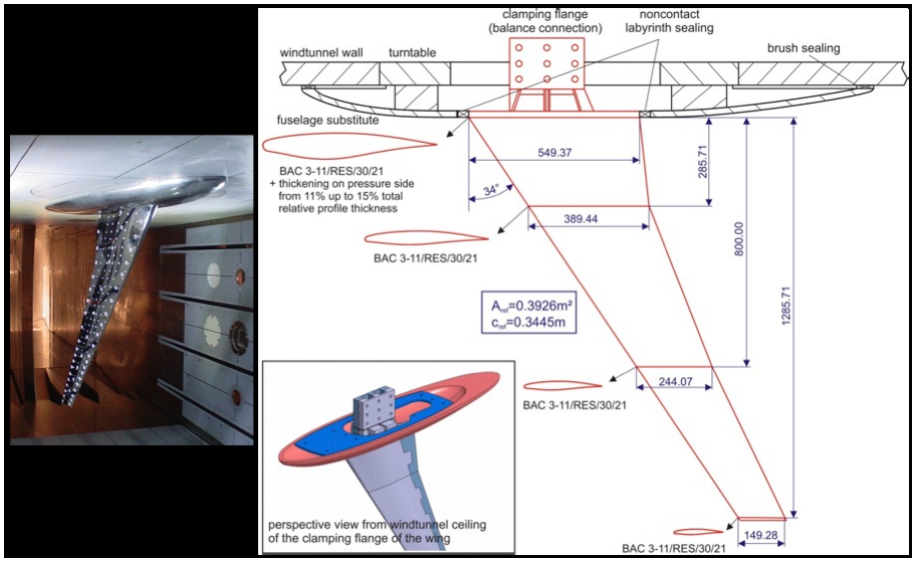

Figure 1: Model planform and assembly of the HIRENASD wing [26].

The steady aeroelastic analysis of the HIRENASD wing is accomplished for the "Low Reynolds Case" [27]. The free vibration analysis is performed in Nastran, and then this modal solution is used as the structural model in the aeroelastic solution by ZEUS. The modal analysis is based on the latest HIRENASD FEM model of NASA, HIRENASD Modeshapes Nov 2011 Model [28]. The aerodynamic mesh is generated in ZEUS by using 164 x 62 x 55 block elements. The convergence of the calculated aerodynamic coefficients is shown in Fig. 2.

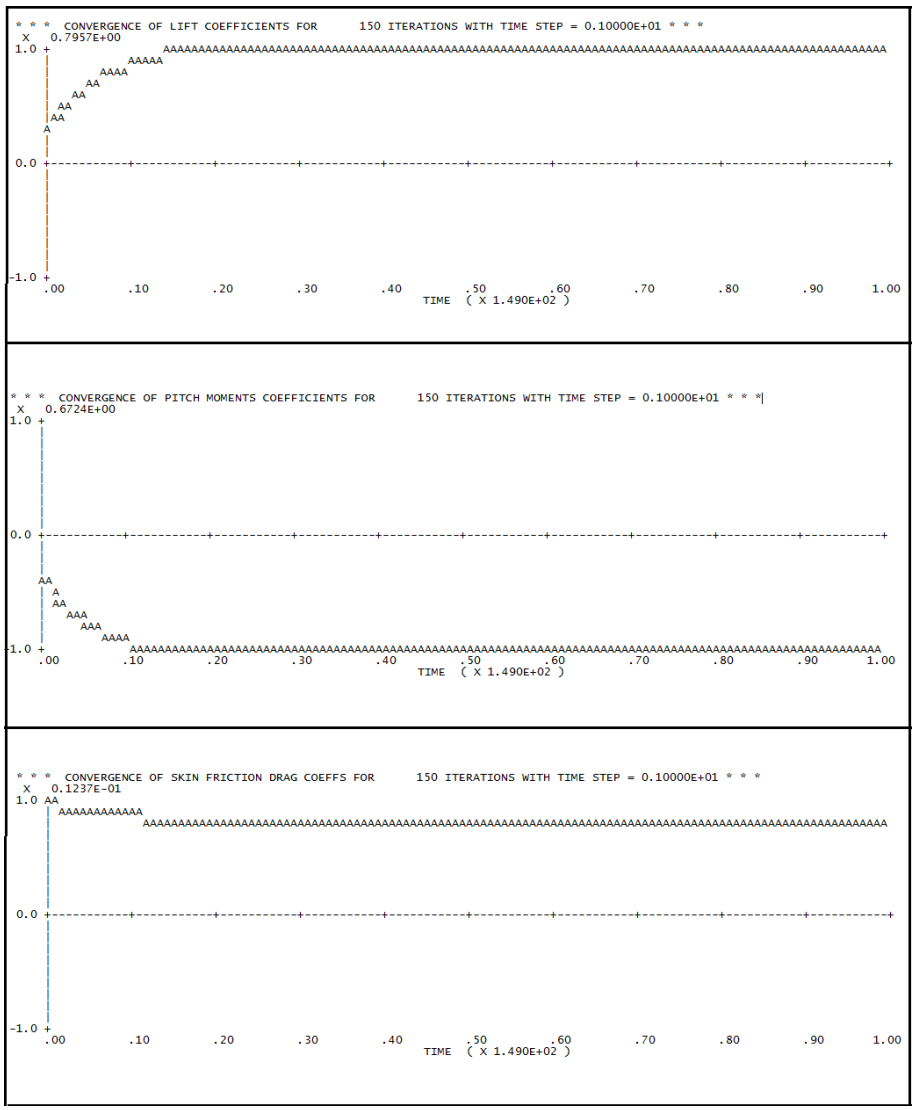

Figure 2: Convergence of aerodynamic coefficients for the HIRENASD wing.

3.2 Static Aeroelastic and Flutter Analyses of the S^{4}T Wing

The second application for the present work relates to the static aeroelastic and flutter analyses of the S^{4}T wing. The S^{4}T wing is a complex aeroelastic semi-span wind-tunnel model, which is designed for aeroelastic/aeroservoelastic analysis [29]. The wind-tunnel model is 16.5 ft in length with a model span of 3.25 ft. The fuselage of the wing consists of a graphite-epoxy flexible beam attached to an aluminum C-channel rigid beam. Fig. 3 shows the wing configuration.

Since a series of wind tunnel tests of the S^{4}T model for the Mach numbers ranging from 0.6 to 1.2 have been performed at NASA Langley Research Center to measure the steady and unsteady characteristics, the output parameters are specified as steady lift, moment and drag coefficients, flutter speed and flutter dynamic pressure to provide comparable computational data for all cases. First, the structural model of NASA is used to perform the modal analysis and then the aerodynamic mesh is constructed in ZEUS (Fig. 4). The size of aerodynamic block mesh (Fig. 5) is 143 x 82 x 78.

The static aeroelastic analysis employs the first 25 structural modes. However, 10 structural

a) S^{4}T structure

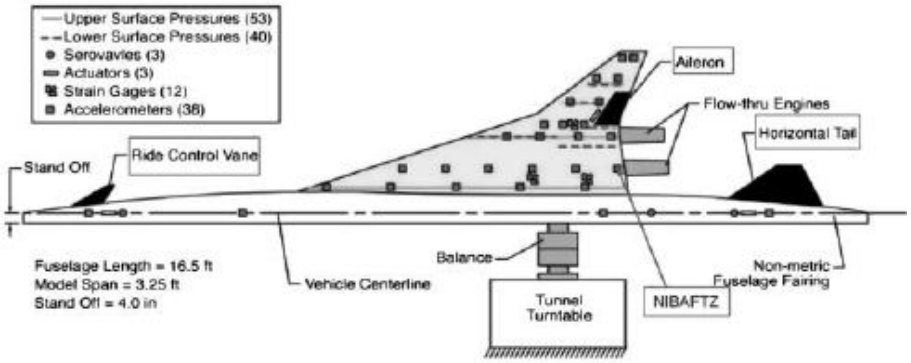

b) Sensor locations of the S^{4}T structure

Figure 3: S^{4}T wing configuration [30].

modes are used in the flutter analysis to reduce the computational time since the flutter analysis takes about 8 hours. The flutter analysis results for the S^{4}T wing cases are summarized in Table 1 while the steady coefficients will be given with the results of the reduced models in Table 3. The variation of flutter dynamic pressure with respect to Mach number is illustrated in Fig. 6.

4 GENERAL CONCEPTS OF ROM METHODS

The reduced modelling strategy is fundamentally based on a disparate approach compared to high-fidelity computational models. In terms of accuracy, the main focus of model reduction is to form an almost equivalent surrogate for computationally expensive models. Acquisition of the reduced models requires few high-fidelity computational analyses depending on the number of specified input parameters, complexity of the high-fidelity models and expected accuracy level. Once the representative model is constructed, further analyses with various values of the input variables can be accomplished via this reduced model. Since an in-house computational code is developed for each model reduction technique introduced by the present work, the computational time significantly decreases compared to the time requirement of the high-fidelity computational models. The model reduction techniques are utilized throughout the present study considering two different applications. The first application focuses on static aeroelastic responses of the HIRENASD wing while the second case relates to both static and flutter analyses of the S^{4}T wing.

In this section, the numerical techniques used to generate a reduced model basis are introduced at first. Then, these methods are verified by using a benchmark problem from literature. Detailed comparison for the accuracy of the PCE and POD based reduced models with the high-fidelity computational analyses clarifies the importance of considered sample number, ap-

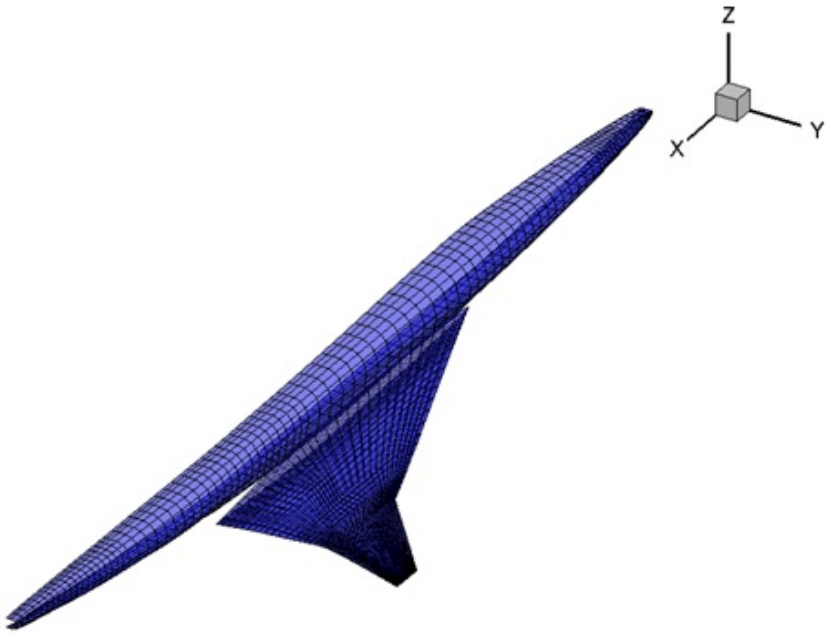

Figure 4: Aerodynamic surface mesh of the S^{4}T wing.

proximation order and computational complexity.

4.1 Polynomial Chaos Expansion (PCE)

Non-intrusive PCE defines a reduced model basis in terms of orthogonal polynomials. In the present study, the Hermite polynomials are used as the orthogonal polynomials. The definition of the first few Hermite polynomials are given below in terms of the standard variable, ξ:

$$H_o(\xi) = 1 \tag{4}$$

$$H_1(\xi) = \xi \tag{5}$$

$$H_2(\xi) = \xi^2 - 1 \tag{6}$$

$$H_3(\xi) = \xi^3 - 3\xi \tag{7}$$

$$H_4(\xi) = \xi^4 - 6\xi^2 + 3 \tag{8}$$

$$H_5(\xi) = \xi^5 - 10\xi^3 + 15\xi \tag{9}$$

$$H_6(\xi) = \xi^6 - 15\xi^4 + 45\xi^2 - 15 \tag{10}$$

The chaos coefficients can be calculated by using the following relation for a two-dimensional system:

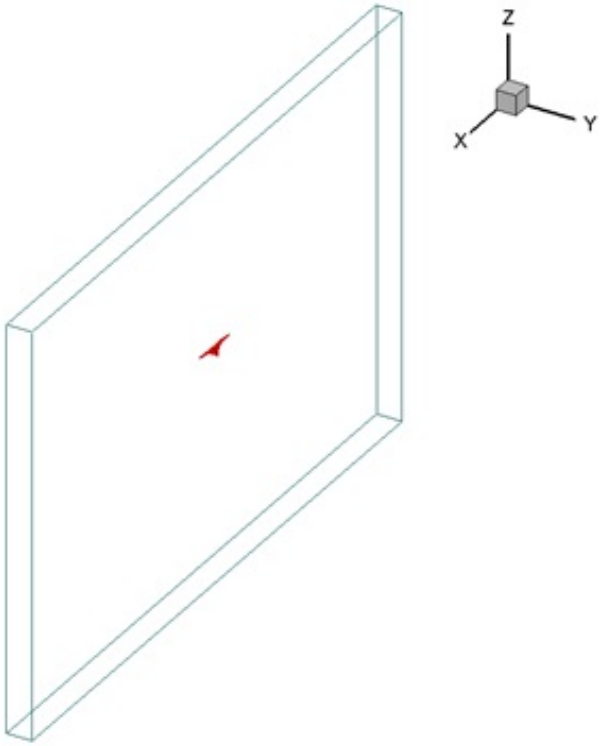

Figure 5: Aerodynamic block element of the S^{4}T wing.

$$\begin{Bmatrix} u_1 \\ u_2 \\ . \\ . \\ u_n \end{Bmatrix} = \begin{bmatrix} H_{01} & H_{11} & . & . & H_{p1} \\ H_{02} & H_{12} & . & . & H_{p2} \\ . & . & . & . & . \\ . & . & . & . & . \\ H_{0n} & H_{1n} & . & . & H_{pn} \end{bmatrix} \begin{Bmatrix} a_1 \\ a_2 \\ . \\ . \\ a_p \end{Bmatrix} \tag{11}$$

where u_i ($i = 1$ to n) is output response which is known from the analyses and a_j ($j = 1$ to p) shows chaos coefficients to be determined. The order of the approximation is denoted by p and n shows the dimension. In this matrix system, the parameters H_{ji} indicate the multiplication of H_j and H_i functions defined in Eq. (4) to (10). However, in two-dimensional case, H_j is the function of the first standard random variable, ξ, while H_i is the function of the second standard random variable, η. The reduced model can be constructed by using the chaos coefficients. In order to calculate the chaos coefficients, linear regression can be applied. Considering the standard normal variables ξ and η, a general linear regression model can be defined in closed form as below:

$$U = H\hat{a} + \varepsilon \tag{12}$$

The regression coefficients, $\hat{a}$, can be computed by using Eq. (13):

$$\hat{a} = (H^T H)^{-1} H^T U \tag{13}$$

M	ρ (slin/in^3)	ω_f (Hz)	Q_f (psf)	U_f (ft/s)	Flutter Mode
0.60	6.958E-8	7.836	79.992	333	2
0.65	5.929E-8	7.809	79.292	360.75	2
0.70	5.112E-8	7.781	78.788	388.50	2
0.75	4.453E-8	7.746	78.420	416.25	2
0.80	3.914E-8	7.709	78.153	444	2
0.85	3.467E-8	7.663	77.960	471.25	2
0.90	3.093E-8	7.592	77.818	499.50	1
0.95	2.603E-8	7.587	75.002	527.25	1
1.05	2.840E-8	7.821	89.986	582.75	2
1.10	2.588E-8	7.832	99.994	610.50	2
1.15	2.723E-8	7.825	114.977	638.25	2
1.20	2.827E-8	7.828	130.003	666	2

Table 1: Flutter results for the S^{4}T wing.

After determining the regression coefficients, the reduced model for the reference initial design can be constructed by using the below relation:

$$U_j(\xi^*, \eta^*) = a_1 H_{0j}(\xi^*, \eta^*) + a_2 H_{1j}(\xi^*, \eta^*) + ... + a_p H_{pj}(\xi^*, \eta^*) \tag{14}$$

where ξ^* and η^* are the values of the standard random variables in the initial design.

4.1.1 Validation of PCE

The PCE method is firstly validated by an example problem [2] which is defined as:

$$z(x,t) = e^{-|(x-0.5)(t-1)|} + \sin(xt), \quad 0 \leq x \leq 1, \;\; 0 \leq t \leq 2 \tag{15}$$

The solution to this function is computed for the uniformly distributed 25 x points and 50 t points. Table 2 shows the relative error values with respect to the order of approximations and the number of samples while the analytical model and the PCE approximations are also plotted together (Fig. 7). The figures correspond to the 100000 samples.

The results conclude that a higher order approximation gives more accurate results. Moreover, the number of samples used to calculate the chaos coefficients significantly affects the accuracy level. Since randomly distributed samples are used in this example, it is quite difficult to determine an optimum sample number for the non-intrusive calculation.

4.2 Proper Orthogonal Decomposition (POD)

POD method is explored to construct reduced models for the static aeroelastic and flutter analyses of the HIRENASD and S^{4}T wings. The present section introduces the general mathematical concepts for the POD method.

The data obtained from any physical model has regularities. The POD is generally used in the presence of regularities in order to reduce the model. In the POD method, the effect of the first mode is the highest and the second mode is less effective than it and so on. The system is defined as a linear combination of independent and orthogonal basis functions. The functions

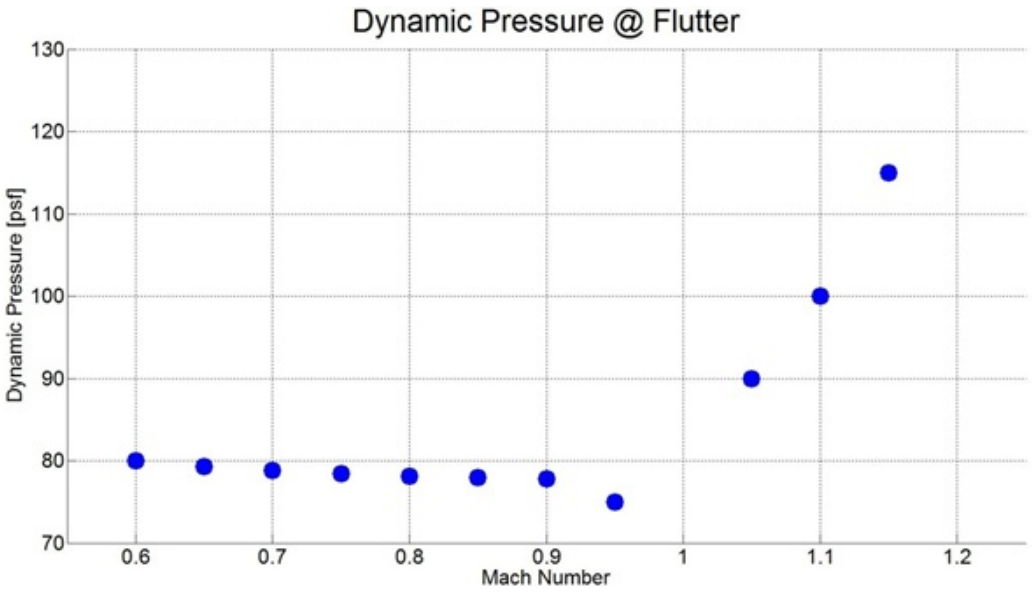

Figure 6: Dynamic pressure - Mach number relation for the S^{4}T wing.

are known as "POD basis functions" and required to represent the reduced model. An *n*th order physical model can be expressed as a linear combination given as below:

$$M = a_1\varphi_1 + a_2\varphi_2 + ... + a_k\varphi_k \tag{16}$$

where *M* is an output response for a snapshot of the variables, a_i are POD coefficients, φ_i are POD basis functions and k is the order of reduced model $(k < n)$. In this study, the "method of snapshots" is used for ROM. This method represents any given physical system with a snapshot matrix with responses representing the basic features of the model. The correlation matrix is defined in terms of the snapshot matrix and the number of POD basis vectors:

$$C = \frac{1}{n}T.T^T \tag{17}$$

where the snapshot matrix, T, is an $n \times m$ matrix (m is number of snapshots) and can be constructed by using the output parameters. The POD basis vectors and coefficients are calculated through the eigenvalues and eigenvectors of the correlation matrix. The number of required POD basis vectors (POD modes) is computed by considering the captured energy from the original model. The total captured energy is defined in Eq. (18).

$$E_{total} = \sum_{i=1}^{n} \lambda_i \tag{18}$$

where λ is normalized eigenvalues of the correlation matrix, C, and n is the required number of POD modes to reach the specified captured energy level. In the present work, the captured energy level is taken 99.9 % in all applications.

The construction of the POD based reduced models requires the use of SVD technique. In this method, the factorization of a real matrix, T is given below:

$$[T]_{k\times p} = [P]_{k\times k}[\Gamma]_{k\times p}[V]^T_{p\times p} \tag{19}$$

Approximation Method	Sample Number	Error
2^{nd} Order PCE	10	13.93%
2^{nd} Order PCE	100	8.00%
2^{nd} Order PCE	1000	7.42%
2^{nd} Order PCE	100000	7.41%
4^{th} Order PCE	10	172.78%
4^{th} Order PCE	100	3.74%
4^{th} Order PCE	1000	3.21%
4^{th} Order PCE	100000	3.18%
6^{th} Order PCE	10	399.71%
6^{th} Order PCE	100	1.61%
6^{th} Order PCE	1000	1.18%
6^{th} Order PCE	100000	1.18%

Table 2: Error values for different order PCE approximations and sample numbers.

where P, the columns of which consist of the eigenvectors of $[T]\,[T]^T$ is left singular vector of T while V, the columns of which consist of the eigenvectors of $[T]^T\,[T]$ is right singular vector of T. $[\Gamma]$ is a diagonal matrix representing the square roots of POD eigenvalues, λ_i. The POD coefficients can be computed by using the relation below:

$$a_i = T^T \cdot \varphi \tag{20}$$

4.2.1 Validation of POD

For validation, the same example problem given in Eq. (16) is considered. Fig. 8 shows the analytical solution and POD solutions for different mode numbers while Table 3 shows the relative error values with respect to the analytical solution for the POD method with different mode numbers and PCE with different orders. The total number of samples is 1250 for all cases in order to compare the POD and PCE methods.

Method	Relative Error
POD (1 mode)	7.94%
POD (2 modes)	5.56%
POD (3 modes)	0.12%
POD (4 modes)	0.029%
POD (5 modes)	0.0005%
PCE (2^{nd} Order)	7.46%
PCE (4^{th} Order)	3.16%
PCE (6^{th} Order)	1.27%

Table 3: Comparison of different ROM techniques for the example problem.

The above table basically indicates that the POD gives quite accurate results beginning from 3 modes. The accuracy level of the PCE is much lower than POD even a higher order approximation is used. The accuracy of the PCE can still be enhanced, however, in this case the

computational procedure will certainly become more complex. On the hand, the accuracy level of the POD can easily be increased if needed since using additional POD modes is just a simple computational step in programming.

5 PCE AND POD BASED ROM FOR STATIC AEROELASTIC ANALYSIS OF THE HIRENASD WING

In the present work, the model reduction techniques are firstly applied to the high-fidelity computational model of the HIRENASD wing. The reduced model depends on the aerodynamic input parameters selected as Mach number and angle of attack while steady lift, drag and moment coefficients are investigated as output static responses. The ROM strategy is based on the 6^{th} order PCE and POD. The PCE and POD calculations are again 2-dimensional since two input variables (angle of attack and Mach number) are specified. 40 generated random design samples are found to provide satisfactory results with respect to the high fidelity static analysis with ZEUS software. These samples are used to construct the PCE and POD based reduced models for static aeroelastic response of the HIRENASD wing for Low Reynolds test conditions. For the PCE based reduced model, Fig. 9-11 illustrate the step-by-step values of the output parameters with respect to the number of design samples while Fig. 12 shows the error values of the output parameters with respect to the sample number. The results of the PCE and POD based reduced models are given by Table 4.

Parameter	Computational	PCE-ROM	PCE Error	POD-ROM	POD Error
c_L	0.3966	0.3982	0.4098%	0.3986	0.5039%
c_D	0.1188	0.1198	0.8027%	0.1190	0.1561%
c_M	-0.6665	-0.6753	1.3144%	-0.6603	0.9345%

Table 4: Results and relative errors for reduced models.

The calculated error values for 40 design samples seem to be sufficient, however, it can be enhanced by the use of more design samples or other sampling methods. The PCE and POD based reduced models give similar results in this application.

6 PCE AND POD BASED ROM FOR STATIC AEROELASTIC AND FLUTTER ANALYSES OF THE S^{4}T WING

The ROM strategy is secondly applied to the high-fidelity computational aeroelastic model of the S^{4}T wing. The 6^{th} order PCE and POD methods are used to represent the static aeroelastic and flutter analyses of the S^{4}T wing. In these studies, the input parameters are defined as Mach number and angle of attack while steady lift, moment and drag coefficients, flutter dynamic pressure and flutter speed are designated as output variables. The random sampling set is generated by considering $M = 0.6$ case where angle of attack varies between -0.3 and 1.0 degrees. 24 design samples are generated to construct the reduced models. Fig. 13-17 show the convergence of the PCE and POD based reduced models to the reference analysis, which was performed for $M = 0.6$ and α=0^o case. The results of the PCE and POD based reduced models and the reference analysis are depicted by Table 5 while the relative error values for the constructed reduced models can be investigated via Table 6. Table 6 clearly shows that the PCE and POD techniques provide sufficient accuracy levels. However, the POD method gives more accurate results as in the static aeroelastic model of the HIRENASD wing.

Method	c_L	c_D	c_M	V_f (ft/s)	Q_f (psf)
Reference	-0.0708834	0.00329277	-0.00392818	332.9993107	79.99559666
PCE-ROM	-0.0737	0.0032	-0.0039	332.9653	79.9801
POD-ROM	-0.0695	0.0034	-0.0039	332.9957	79.9928

Table 5: Results of reference analysis, and PCE and POD based ROMs for the S^{4}T wing.

Method	Error of c_L	Error of c_D	Error of c_M	Error of V_f	Error of Q_f
PCE	3.974 %	2.817 %	0.717%	0.010%	0.019%
POD	1.952%	3.257%	0.717%	0.001%	0.003%

Table 6: Relative error values of the PCE and POD methods for the S^{4}T wing.

7 CONCLUSIONS AND FUTURE WORK

The present work introduces reduced modelling strategy based on PCE and POD techniques. The model reduction is performed to represent the high-fidelity computational aeroelastic analyses of the HIRENASD and S^{4}T wings. First, the initial high-fidelity aeroelastic analyses are accomplished by using Nastran and ZEUS software. After the construction of the PCE and POD based reduced models, the reference aeroelastic analyses are also performed via these models. Both the PCE and POD methods give satisfactory results. However, the POD method is just a step ahead in terms of accuracy.

For future work, the computational efficiency of the reduced models can be exploited more. For instance, instead of using high-fidelity computational models, the structural and aerodynamic uncertainties may be quantified through the reduced models to save computational time.

REFERENCES

[1] P. C. Chen, Z. Zhang, A. Sengupta and D. Liu, Overset Euler/Boundary Layer Solver with Panel Based Aerodynamic Modeling for Aeroelastic Applications. *Journal of Aircraft*, Vol. 46, No. 6, pp. 2054-2068, 2009.

[2] N. Wiener, The homogenous chaos. *American Journal of Mathematics*, Vol. 60, pp: 897-936, 1938.

[3] M. S. Eldred, Recent Advances in Non-Intrusive Polynomial Chaos and Stochastic Collocation Methods for Uncertainty Analysis and Designs. *50th AIAA/ASME/ASCE/AHS/ASC Structures, Structural Dynamics, and Materials Conference*, AIAA 2009-2274, Palm Springs, California, USA, 2009.

[4] M. S. Eldred and J. Burkardt, Comparision of Non-Intusive Polynomial Chaos and Stochastic Collocation Methods for Uncertainty Quantification. *47th AIAA Aerospace Sciences Meeting and Exhibit*, AIAA 2009-0976, Orlando, FL, USA, 2009.

[5] J. A. S. Witteveen and H. Bijl, Using Polynomial Chaos for Uncertainty Quantification in Problems with Nonlinearities. *47th AIAA/ASME/ASCE/AHS/ASC Structures, Structural Dynamics, and Materials Conference*, AIAA 2006-2066, Newport, Rhode Island, USA, 2006.

[6] P. Beran and W. Silva, Reduced Order Modeling: New Approaches to Computational Physics. *39th AIAA Aerospace Sciences Meeting and Exhibit*, AIAA 2001-0853, Reno, NV, USA, 2001.

[7] R. G. Ghanem and P. D. Spanos, Stochastic Finite Element Methods: A spectral Approach. Springer-Verlag, 1991.

[8] K. Karhunen, Zur Spektraltheorie stochastischer Prozesse. *Ann. Acad. Sci. Fennicae. Ser. A. I. Math.-Phys.*, 1946 (34): 7, 1946.

[9] M. Loeve, Fonctions aleatoire de second ordre. *Revue*, 48: 195-206, 1946.

[10] H. Hoetelling, Simplified calculation of principal component analysis. *Psychometrica*, 1: 27-35, 1935.

[11] T. Bui-Thanh and K. Willcox, Model Reduction for Large Scale CFD Applications Using the Balanced Proper Orthogonal Decomposition. *17th AIAA Computational Fluid Dynamics Conference*, AIAA 2005-4617, Toronto, Canada, 2005.

[12] P. A. LeGresley and J. Alonso, Investigation of Non-Linear Projection for POD Based Reduced Order Models for Aerodynamics. *39th AIAA Sciences Meeting and Exhibit*, AIAA 2001-0926, Reno, NV, USA, 2001.

[13] K. C. Hall, J. P. Thomas and E. H. Dowell, Investigation of Non-Linear Proper Orthogonal Decomposition Technique for Transonic Unsteady Aerodynamic Flows. *AIAA Journal*, Vol. 38, No. 10, pp: 1853-1862, 2000.

[14] J. P. Thomas, E. H. Dowell and K. C. Hall, Three-Dimensional Transonic Aeroelasticity Using Proper Orthogonal Decomposition-Based Reduced-Order Models. *Journal of Aircraft*, Vol. 40, No. 3, pp: 544-551, 2003.

[15] T. Lieu and M. Lesoinne, Parameter Adaptation of Reduced Order Models for Three-Dimensional Flutter Analysis. *42nd AIAA Aerospace Sciences Meeting and Exhibit*, AIAA 2004-888, Reno, Nevada, USA, 2004.

[16] M. Allen, G. Weickum and K. Maute Application of Reduced Order Models for the Stochastic Design Optimization of Dynamic Systems. *10th AIAA/ISSMO Multidisciplinary Analysis and Optimization Conference*, AIAA 2004-4614, Albany, NY, USA, 2004.

[17] R. F. Coelho, P. Breitkopf and C. Knopf-Lenoir, Model reduction for multidisciplinary optimization - application to a 2D wing. *Structural and Multidisciplinary Optimization*, Vol. 37, No. 1, pp: 29-48, 2008.

[18] A. Chatterjee, An Introduction to the Proper Orthogonal Decomposition. *Current Science-Bangalore*, Vol. 78, No. 7, pp: 808-817, 2000.

[19] R. Pinnau, Model Reduction via Proper Orthogonal Decomposition. *Model Order Reduction: Theory, Research Aspects and Applications*, Springer, 2008.

[20] B. Zhang, Y. Lian and W. Shyy, Proper Orthogonal Decomposition for Three-Dimensional Membrane Wing Aerodynamics. *33rd AIAA Fluid Dynamics Conference and Exhibit*, AIAA 2003-3917, Orlando, FL, 2003.

[21] M. Xiao, P. Breitkopf and R. F. Coelho, Model Reduction by CPOD and Kriging Application to the Shape Optimization of an Intake Port. *Structural and Multidisciplinary Optimization*, 41 (4), 555-574, 2010.

[22] L. Sirovich, Turbulence and the dynamics of coherent structures. IIII. *Quart. Appl. Math.*, Vol. 45, No. 3, pp: 561-590, 1987.

[23] ZEUS: A CFD Code for Aeroelasticians User Manual, Version 3.2, Zona Technology, February 2012.

[24] A. Jameson, W. Schmidt, E. Turkel, Numerical Solution of the Euler Equations by Finite Volume Methods Using Runge Kutta Time Stepping Schemes, AIAA 81-1259, 1981.

[25] J. Ballmann, A. Boucke, B. H. Chen, L. Reimer, A. Dafnis, S. Bsing and C. Buxel, Aero-Structural Wind Tunnel Experiments with Elastic Wing Models at High Reynolds Number (HIRENASD - ASDMAD. *International Forum on Aeroelasticity and Structural Dynamics (IFASD)*, IFASD 2011-105, Paris, France, 2011.

[26] P. Chwalowski, J. P. Florance, J. Heeg, C. D. Wieseman, B. Perry, Preliminary Computational Analysis of the HIRENASD Configuration in Preparation for the Aeroelastic Prediction Workshop. *International Forum of Aeroelasticity and Structural Dynamics (IFASD)*, IFASD 2011-108, Paris, France, 2011.

[27] M. Nikbay, P. Acar, C. Kilic and Z. Zhang, Steady and Unsteady Aeroelastic Computations of HIRENASD Wing for Low and High Reynolds Numbers. *Presented in 1st Aeroelastic Prediction Workshop (AePW-1)*, Honolulu, HI, USA, 2012.

[28] ”https://c3.nasa.gov/dashlink/resources/489/”, March 2013.

[29] B. Perry, W. A. Silva, J. R. Florance, C. D. Wieseman, A. S. Pototzky, M. D. Sanetrik, et al., Plans and Status of Wind-Tunnel Testing Employing an Aeroservoelastic Semispan Model. *48th AIAA/ASME/ASCE/AHS/ASC Structures, Structural Dynamics, and Materials Conference*, AIAA 2007-1770, Honolulu, HI, USA, 2007.

[30] J. Zeng, S. L. Kukreja and B. Moulin Experimental Model-Based Aeroelastic Control for Flutter Suppression and Gust-Load Alleviation. *Journal of Guidance, Control, and Dynamics*, Vol. 35, No. 5, pp. 1377-1390, 2012.

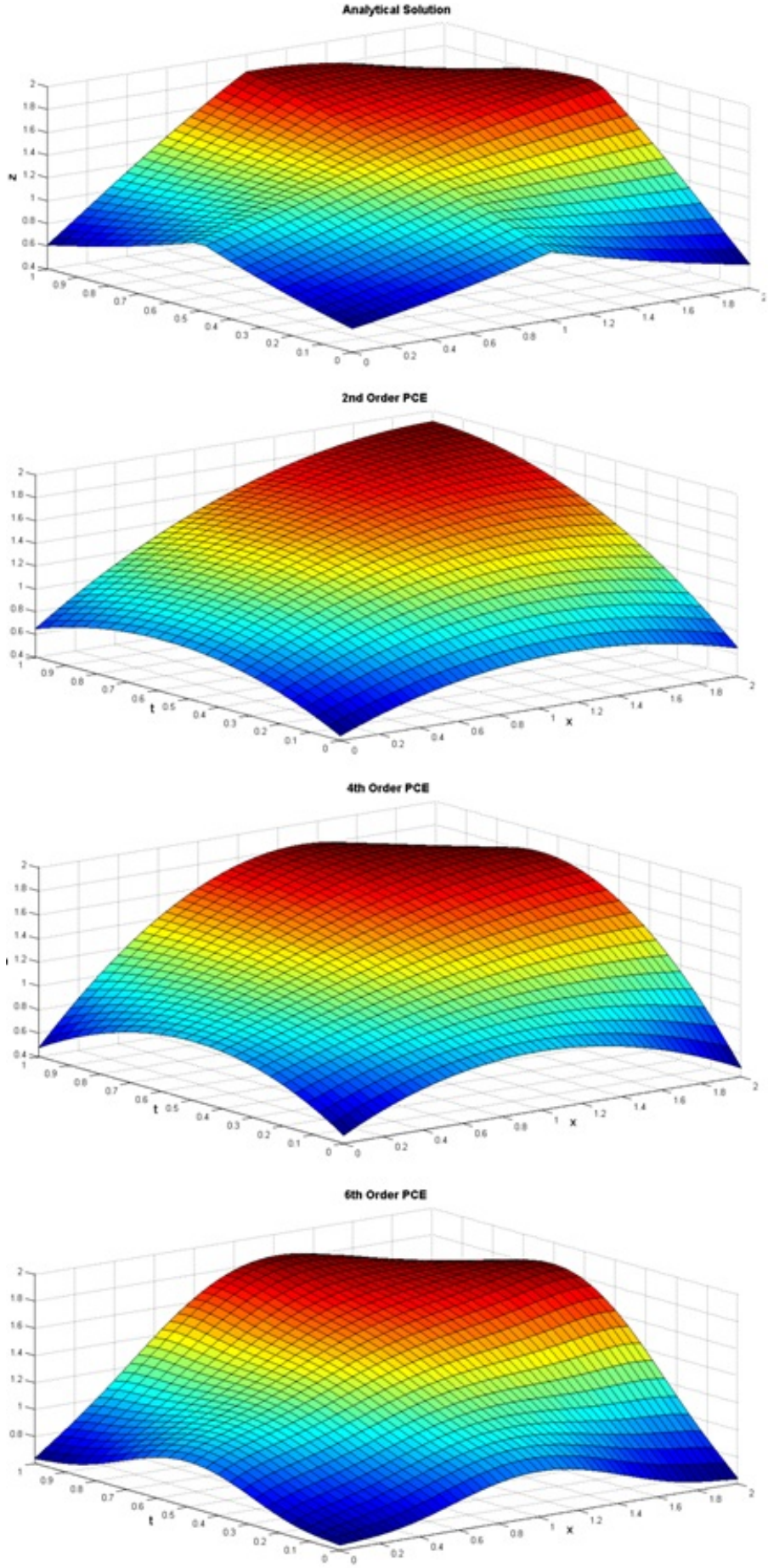

Figure 7: Comparison of analytical solution and PCE results.

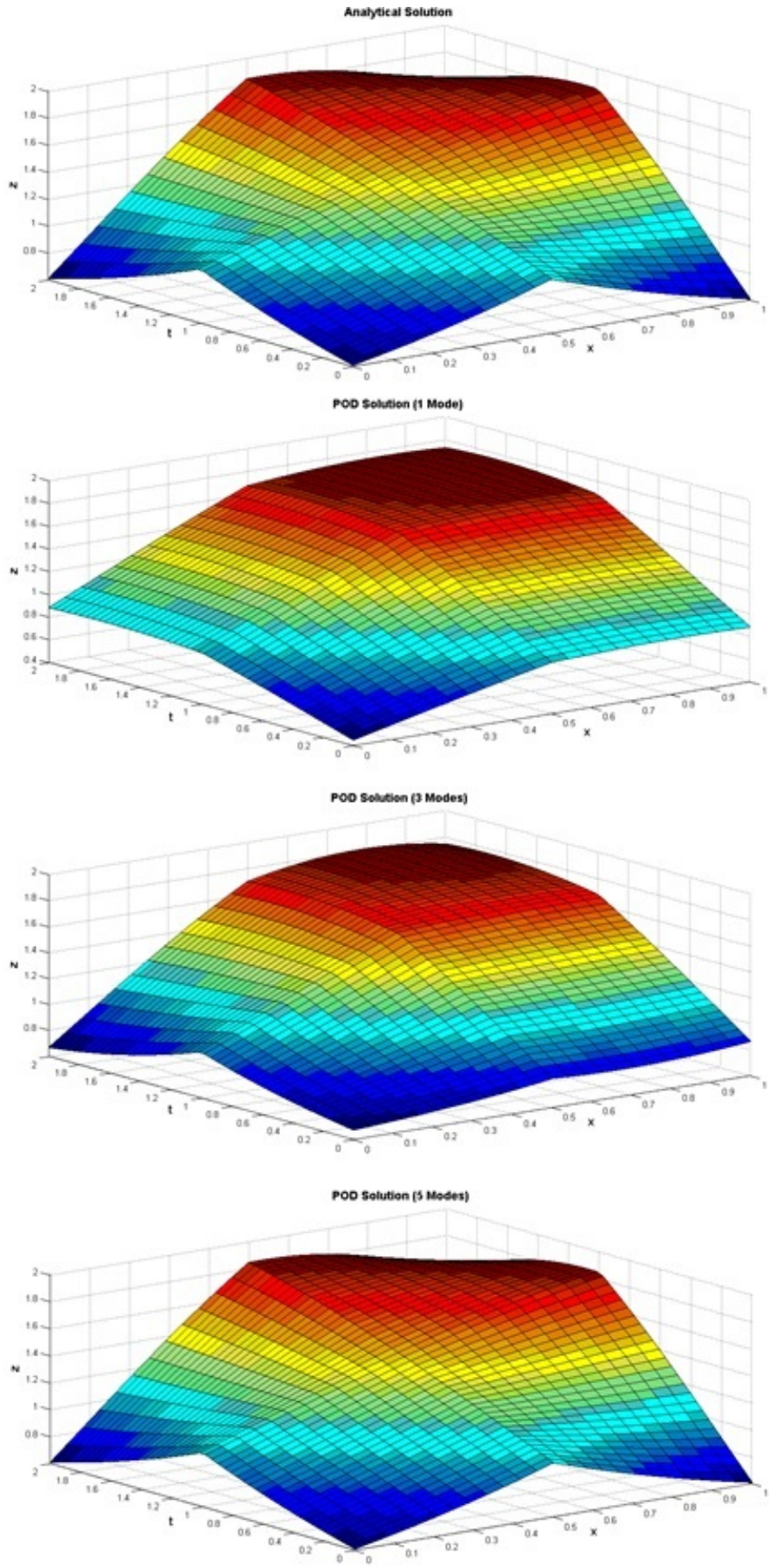

Figure 8: Comparison of analytical solution and POD results.

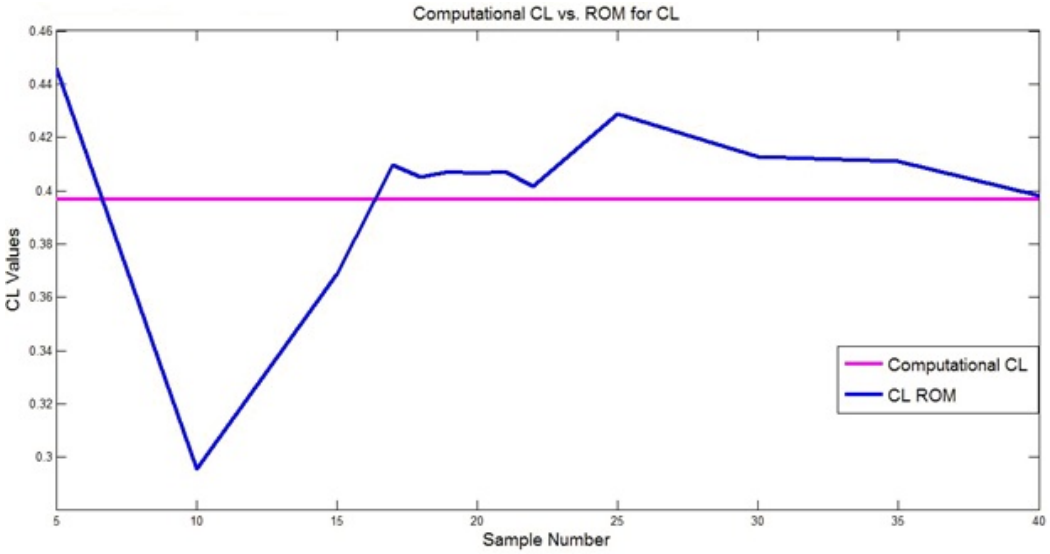

Figure 9: c_L variation of the HIRENASD PCE-ROM with respect to sample number.

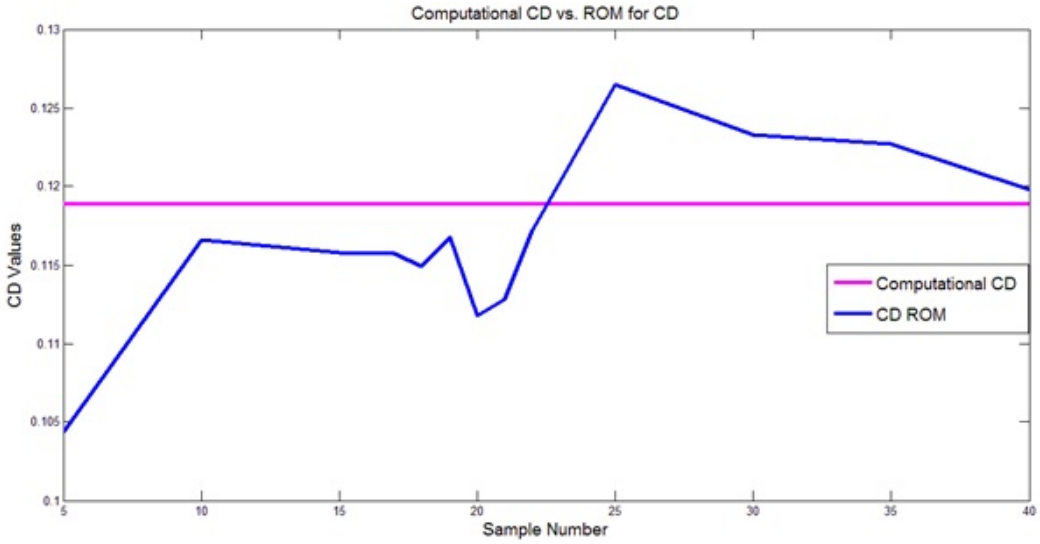

Figure 10: c_D variation of the HIRENASD PCE-ROM with respect to sample number.

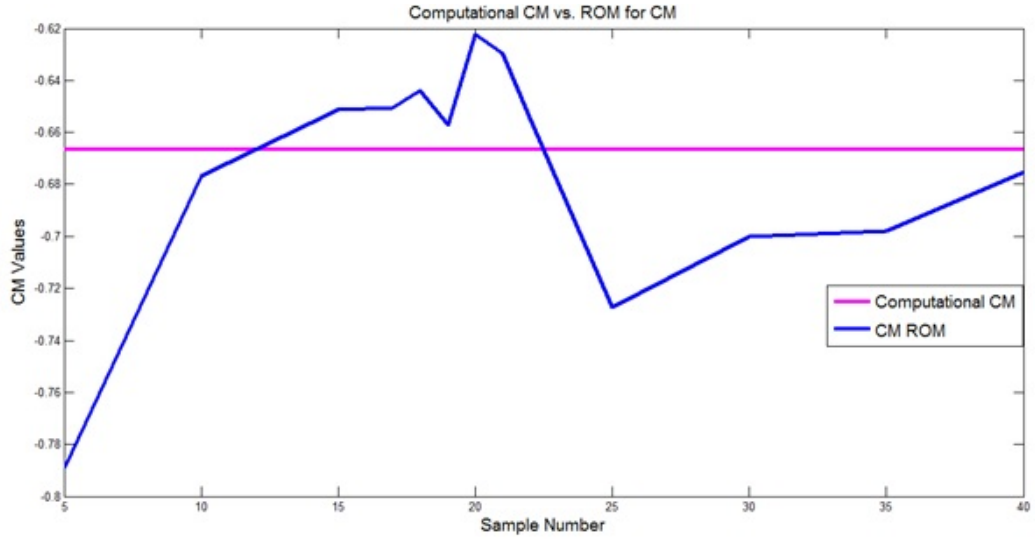

Figure 11: c_M variation of the HIRENASD PCE-ROM with respect to sample number.

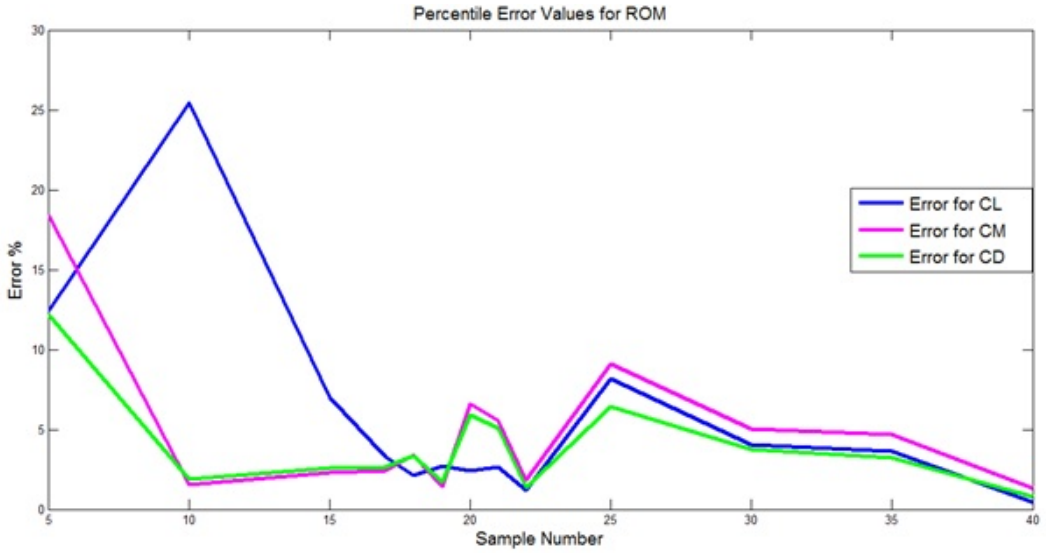

Figure 12: Relative error values for the HIRENASD PCE-ROM with respect to sample number.

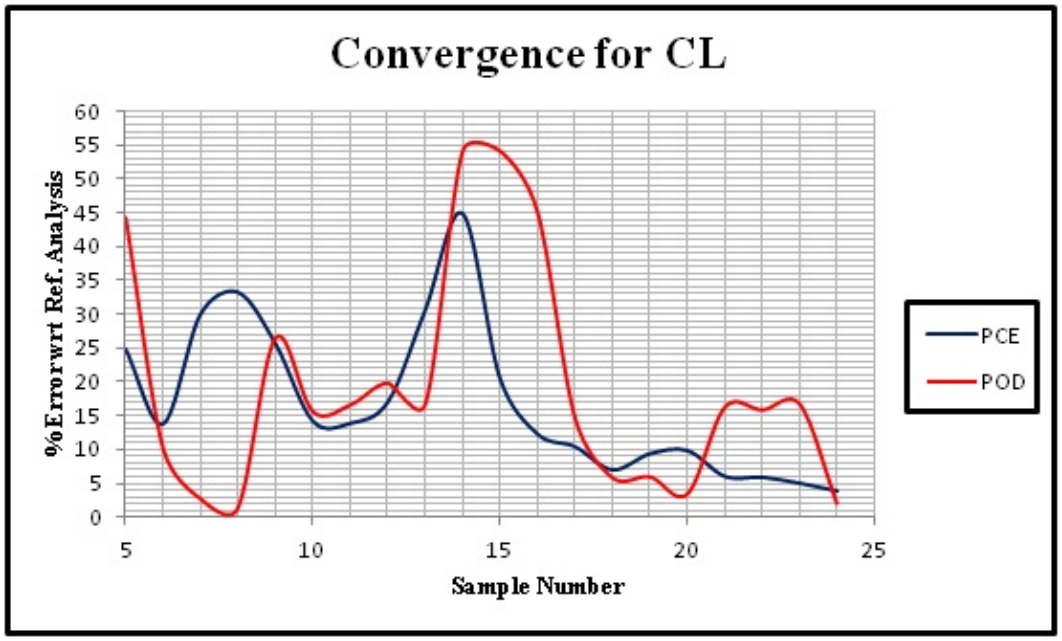

Figure 13: Convergence of the S^{4}T PCE and POD methods for c_L parameter with respect to sample number.

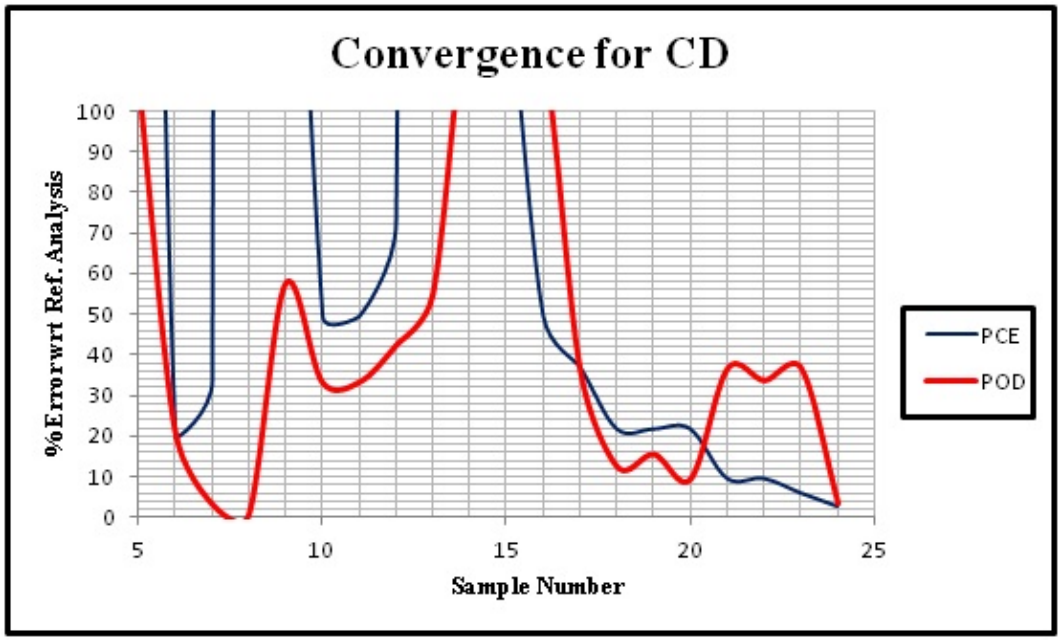

Figure 14: Convergence of the S^{4}T PCE and POD methods for c_D parameter with respect to sample number.

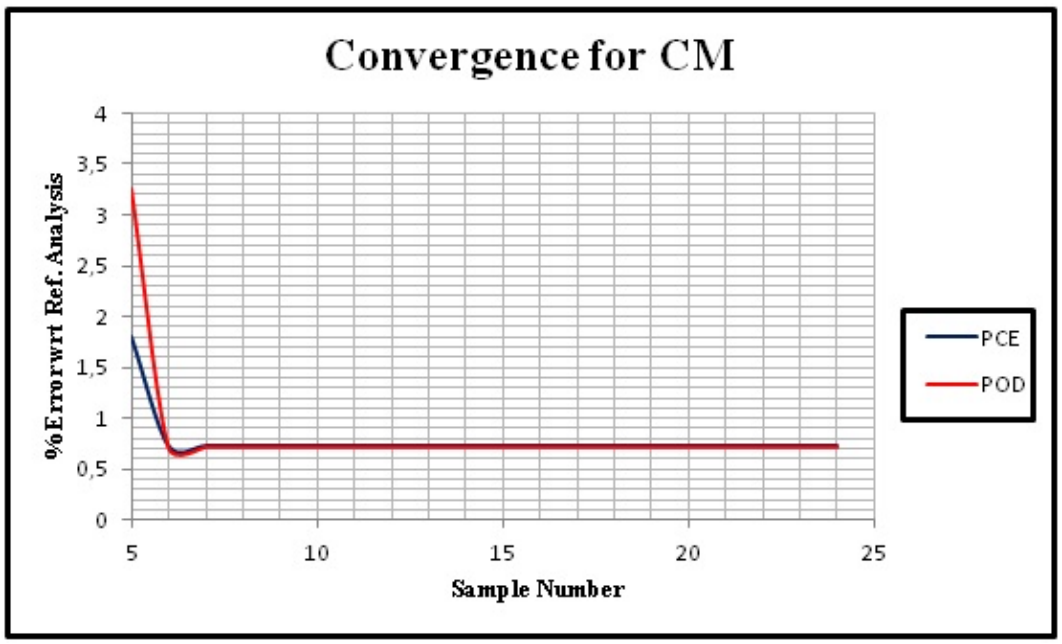

Figure 15: Convergence of the S^{4}T PCE and POD methods for c_M parameter with respect to sample number.

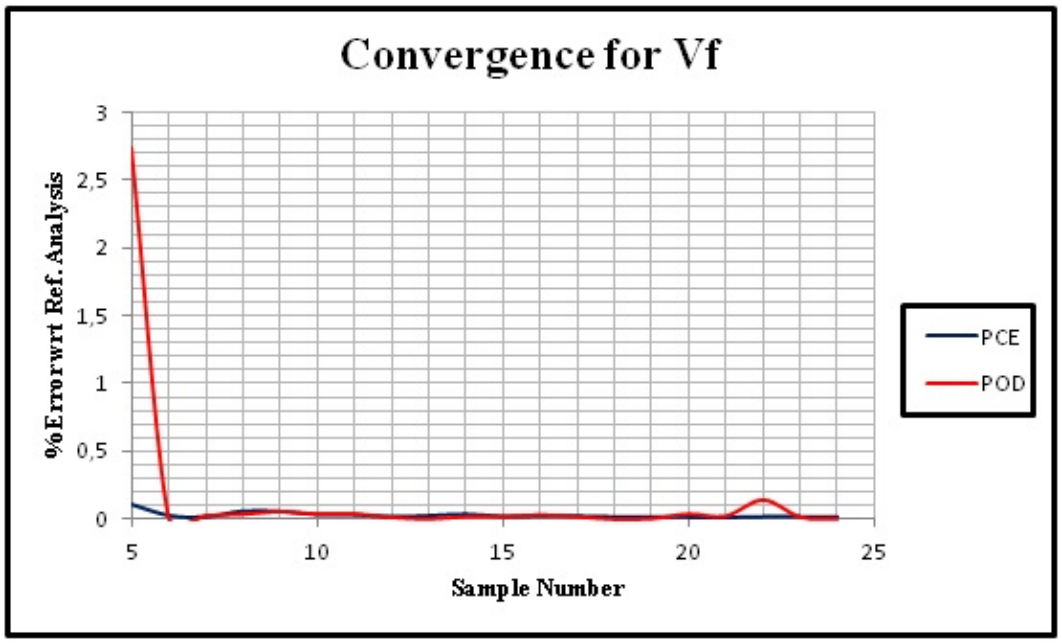

Figure 16: Convergence of the S^{4}T PCE and POD methods for V_f parameter with respect to sample number.

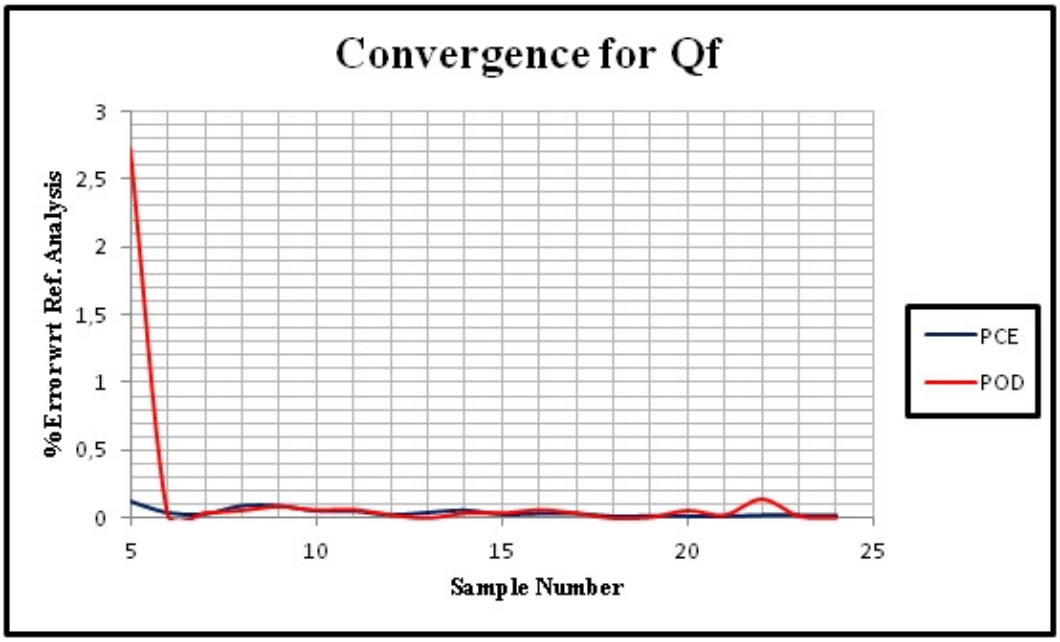

Figure 17: Convergence of the S^{4}T PCE and POD methods for Q_f parameter with respect to sample number.